IEEE Access
Multidisciplinary | Rapid Review | Open Access Journal

Date of publication xxxx 00, 0000, date of current version xxxx 00, 0000.

Digital Object Identifier 10.1109/ACCESS.2017.Doi Number

Electromechanical Equivalent Circuit Model of a Piezoelectric Disk Considering Three Internal Losses

Xiaoxiao Dong[1], Kenji Uchino[2], (Fellow, IEEE), Chunrong Jiang[3], Long Jin[4], Zhike Xu[4], and Yue Yuan[1]

[1] College of Energy and Electrical Engineering, Hohai University, Nanjing 211100 China
[2] International Center for Actuators and Transducers, The Pennsylvania State University, University Park, PA 16802 USA
[3] College of Electric Power Engineering, Nanjing Institute of Technology, Nanjing 211167 China
[4] College of Electrical Engineering, Southeast University, Nanjing 210098 China

Corresponding author: Xiaoxiao Dong (e-mail: dongxiaoxiao@hhu.edu.cn).

This work was supported in part by the Fundamental Research Funds for the Central Universities under Grant 2018B06914, and in part by the National Natural Science Foundation of China under Grant 51777029.

ABSTRACT Heat generation by internal loss factors of piezoelectrics is one of the critical issues for high power density piezoelectric applications, such as ultrasonic motors, piezoelectric actuators and transducers. There are three types of internal losses in piezoelectric materials, namely dielectric, elastic and piezoelectric losses. In this paper, a decoupled equivalent circuit is proposed to emulate a piezoelectric disk in radial vibration mode considering all three types of internal losses. First, the decoupled equivalent circuit is derived according to the conventional electromechanical equivalent circuit model. Then, a piezoelectric disk configuration in radial vibration mode is explored and simulated. The resonance and antiresonance frequencies and their corresponding mechanical quality factors are achieved by the proposed circuit. In order to verify the accuracy of the simulation results, the piezoelectric disk is fabricated and tested. Simulation results with the new circuit exhibit a good agreement with experimental results. Finally, the equivalent circuit with only dielectric and elastic losses are simulated and compared which further validates the accuracy improvement of the new equivalent circuit considering all three losses.

INDEX TERMS Piezoelectric material, equivalent circuit, radial vibration, loss factor, piezoelectric loss

I. INTRODUCTION

Piezoelectric ultrasonic motors have developed rapidly since the 1980s, due to the superiority of high efficiency in the mm-size motor area [1-3]. The bottleneck of piezoelectric ultrasonic motors has been identified as heat generation, which is a significant problem for high power density applications [4]. Internal losses in piezoelectric materials are considered in general to have three different mechanisms, namely dielectric, mechanical, and piezoelectric losses [5]. Accurate determination of three types of losses is critical, since they are closely related to the heat generation mechanism in piezoelectrics.

Mechanical quality factors are basically related to the three types of losses and play a significant role in the study of heat generation of piezoelectric devices [6]. A higher mechanical quality factor reduces the heat generation and increases the efficiency. Electromechanical equivalent circuit (EC) model is one of the most effective method to analyze the properties of piezoelectric vibrator [7-9]. IEEE Standard only provides a method to obtain the mechanical quality factor (Q_m) at resonance frequency according to an EC model [10]. However, the main issue of this standard method is that it assumes piezoelectric loss to be the average value of elastic and dielectric losses, which results in the equivalence of Q values at resonance and antiresonance. This conclusion is proved to be inaccurate because experimental results indicate there exists a conspicuous discrepancy between the mechanical quality factors at the resonance (Q_R) and the antiresonance (Q_A) in lead-zirconate-titanate (PZT)-based ceramics [11-13]. In recent, the equivalent circuit of piezoelectrics for k_{31} vibration mode considering all three losses have been proposed by researchers at Pennsylvania State University [14], which explains the variation of the mechanical quality factor between resonance and

This article has been accepted for publication in a future issue of this journal, but has not been fully edited. Content may change prior to final publication. Citation information: DOI 10.1109/ACCESS.2020.3028698, IEEE Access

antiresonance frequencies. Further, a six-terminal EC of a ring-type piezoelectrics is proposed including three types of losses, which is utilized in characteristic analysis of an ultrasonic motor [15].

The piezoelectric disk of radial vibration mode is widely used as a vibrator for piezoelectric ultrasonic motors and transducers due to its large power density [16]. Although EC models of k_p vibration mode reported in existing literatures is efficient for analyzing the resonance and antiresonance frequencies [17-19], it is insufficient to achieve accurate mechanical quality factors without considering all three losses in piezoelectrics. In this paper, a decoupled EC of a piezoelectric disk in radial vibration mode is firstly derived considering all three types of internal losses. Based on the proposed electromechanical EC model, mechanical quality factors at resonance and antiresonance frequencies are calculated as a function of three types of losses. In addition, the relationship between frequencies and material properties of the piezoelectric disk is discussed to facilitate the designing of piezoelectric vibrators. Finally, the simulation results obtained from the EC model are compared with and verified by experimental results.

II. ELECTROMECHANICAL EQUIVALENT CIRCUIT OF A PIEZOELECTRIC DISK

A. CONVENTIONAL EQUIVALNET CIRCUIT WITHOUT LOSSES

The configuration of a piezoelectric disk in radial vibration mode is shown in Figure 1. The piezoelectric ceramic thin disk is polarized in its thickness direction and the electrode areas are applied on its upper and lower surfaces. The radial vibration mode is excited by applying an AC voltage at the electrode areas. The conventional electromechanical EC of the piezoelectric disk is shown in Figure 2 [20].

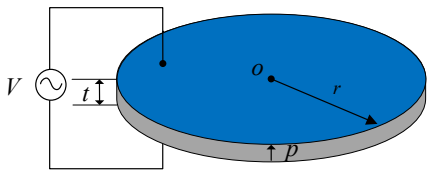

FIGURE 1. Schematic view of a piezoelectric disk.

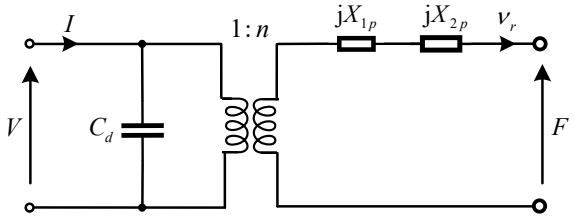

Figure 2. Conventional electromechanical equivalent circuit of the piezoelectric disk.

In Figure 2, V and I denote the input voltage and current in the electrical branch (i.e., the primary side of the equivalent transformer), respectively. F is the output force and v_r is the vibration velocity in the mechanical branch (i.e., the secondary side of the equivalent transformer). C_d is the damped capacitance expressed as

$$C_d = \frac{S}{t}[\varepsilon_{33}^T - \frac{2d_{31}^2}{s_{11}^E(1-\sigma)}] \tag{1}$$

in which ε_{33}^T represents the absolute dielectric permittivity under constant stress; the Poisson's ratio σ is expressed by $\sigma = -s_{12}^E / s_{11}^E$; s_{11}^E and s_{12}^E stand for the elastic compliance under constant electric field, and d_{31} denotes the piezoelectric constant; The area of the end of the piezoelectric disk can be described as $S = \pi r^2$; r is the radius; t is the disk thickness.

The force factor n is the electromechanical conversion coefficient of the piezoelectric disk in radial vibration and expressed as

$$n = 2\pi r \cdot \frac{d_{31}}{s_{11}^E(1-\sigma)} \tag{2}$$

In the mechanical branch, X_{1p} and X_{2p} are impedances described as

$$X_{1p} = -\rho v_p S_r \frac{J_0(kr)}{J_1(kr)} \tag{3}$$

$$X_{2p} = \frac{\rho v_p S_r (1-\sigma)}{kr} \tag{4}$$

Here, ρ is the density; S_r is the area of the side of the piezoelectric disk expressed as $S_r = 2\pi rt$; J_0 and J_1 are Bessel functions of the first kind; the wave number k is expressed by $k = \omega / v_p$; ω stands for the angular frequency; v_p represents the sound velocity and is expressed as

$$v_p = \sqrt{\frac{1}{\rho s_{11}^E} \cdot \frac{1}{1-\sigma^2}} \,. \tag{5}$$

B. EQUIVALENT CIRCUIT WITH THE INTEGRATION OF THREE TYPES OF LOSSES

The heat dissipation in the piezoelectric disk is generally originated from three types of loss factors: dielectric ($\tan\delta_{33}^{'}$), mechanical ($\tan\phi_{11}^{'}$, $\tan\phi_{12}^{'}$), and piezoelectric ($\tan\theta_{31}^{'}$) losses. Losses are integrated into the conventional electromechanical EC by complex parameters expressed as

$$\boldsymbol{\varepsilon_{33}^T} = \varepsilon_{33}^T(1 - \mathrm{j}\tan\delta_{33}^{'}) \tag{6}$$

$$\boldsymbol{s_{11}^E} = s_{11}^E(1 - \mathrm{j}\tan\phi_{11}^{'}) \tag{7}$$

$$\boldsymbol{s_{12}^E} = s_{12}^E(1 - \mathrm{j}\tan\phi_{12}^{'}) \tag{8}$$

$$\boldsymbol{d}_{31} = d_{31}(1 - \mathrm{j}\tan\theta_{31}^{'}) \tag{9}$$

$$\boldsymbol{\sigma} = \sigma\left(1 - \mathrm{j}\left(\tan\phi_{12}^{'} - \tan\phi_{11}^{'}\right)\right) \tag{10}$$

where j is the imaginary notation. It is notable that the loss factors are very small (less than 10%), and therefore imaginary parts can be assumed as $\tan\delta_{33}^{'} \approx \delta_{33}^{'}$, $\tan\phi_{11}^{'} \approx \phi_{11}^{'}$, $\tan\phi_{12}^{'} \approx \phi_{12}^{'}$ and $\tan\theta_{31}^{'} \approx \theta_{31}^{'}$, respectively.

This article has been accepted for publication in a future issue of this journal, but has not been fully edited. Content may change prior to final publication. Citation information: DOI 10.1109/ACCESS.2020.3028698, IEEE Access

Considering complex parameters in the electrical branch of the conventional EC, the damped capacitance in (1) is rewritten as

$$\boldsymbol{C}_d = \frac{S}{t}\left(\boldsymbol{\varepsilon}_{33}^{T} - \frac{2\boldsymbol{d}_{31}^{\,2}}{\boldsymbol{s}_{11}^{E}(1-\boldsymbol{\sigma})}\right) = C_d + \frac{1}{\mathrm{j}\omega R_d} \tag{11}$$

where the damped capacitance C_d denotes the electrical energy storage; R_d represents the extensive dielectric loss derived in the following form,

$$\frac{1}{R_d} = \frac{\omega S}{t}\left(\varepsilon_{33}^{T}\delta_{33}^{'} + \frac{2d_{31}^{\,2}}{s_{11}^{E}(1-\sigma)^2}\cdot\left(\phi_{11}^{'} - \sigma\phi_{12}^{'} - 2\theta_{31}^{'}(1-\sigma)\right)\right) \tag{12}$$

Similarly, the force factor in (2) is rewritten by complex parameters as

$$\boldsymbol{n} = 2\pi r\cdot\frac{\boldsymbol{d}_{31}}{\boldsymbol{s}_{11}^{E}(1-\boldsymbol{\sigma})} = n(1-\mathrm{j}\alpha) \tag{13}$$

Here, α is the phase shift derived as

$$\alpha = \theta_{31}^{'} - \frac{\phi_{11}^{'} - \sigma\phi_{12}^{'}}{1-\sigma} \tag{14}$$

In the mechanical branch, the sound velocity is adjusted as

$$\boldsymbol{v}_p = \sqrt{\frac{1}{\rho\boldsymbol{s}_{11}^{E}}\cdot\frac{1}{1-\boldsymbol{\sigma}^2}} = v_p(1+\mathrm{j}\gamma) \tag{15}$$

where

$$\gamma = \frac{1+\sigma^2}{2(1-\sigma^2)}\phi_{11}^{'} - \frac{\sigma^2}{1-\sigma^2}\phi_{12}^{'} \tag{16}$$

The wave number $\boldsymbol{k}$ can be expressed by the sound velocity as

$$\boldsymbol{k} = \frac{\omega}{\boldsymbol{v}_p} = k(1-\mathrm{j}\gamma) \tag{17}$$

Further, impedances in (3) and (4) can be rewritten as

$$\boldsymbol{Z}_{1p} = R_{1p} + \mathrm{j}X_{1p} \tag{18}$$

$$\boldsymbol{Z}_{2p} = R_{2p} + \mathrm{j}X_{2p} \tag{19}$$

Here, the resistors R_{1p} and R_{2p} denote the mechanical losses; the reactors X_{1p} and X_{2p} represent the mechanical energy storage. It is notable that X_{1p} attributes to motional capacitor (i.e., elasticity), while the reactor X_{2p} attributes to inductor (i.e., mass). In order to clarify the physical meaning of the real and imaginary parts, the complex parameters are decoupled utilizing the properties of Bessel functions as

$$\frac{d}{d(kr)}[(kr)^n J_n(kr)] = (kr)^n J_{n-1}(kr) \tag{20}$$

$$J_{-n}(kr) = (-1)^n J_n(kr) \tag{21}$$

Therefore,

$$\frac{d}{d(kr)}[J_0(kr)] = -J_1(kr) \tag{22}$$

$$\frac{d}{d(kr)}[J_1(kr)] = J_0(kr) - \frac{1}{kr}J_1(kr) \tag{23}$$

Then, applying the Taylor expansions yields

$$\boldsymbol{J_0(kr)} = J_0(kr) + \mathrm{j}kr\gamma J_1(kr) \tag{24}$$

$$\boldsymbol{J_1(kr)} = J_1(kr) - \mathrm{j}kr\gamma\left[J_0(kr) - \frac{1}{kr}J_1(kr)\right] \tag{25}$$

In order to simplify the equations, the first order approximations are used by neglecting higher order terms with respect to small loss factors. Therefore, the resistances in (18) and (19) are derived as

$$R_{1p} = \rho v_p S_r \gamma kr\left(1 + \frac{J_0^{\,2}(kr)}{J_1^{\,2}(kr)}\right) \tag{26}$$

$$R_{2p} = -\rho v_p S_r \cdot \frac{2\gamma(1-\sigma) + \sigma\left(\phi_{12}^{'} - \phi_{11}^{'}\right)}{kr} \tag{27}$$

According to the derivation above, the new decoupled electromechanical EC model of the piezoelectric disk considering three types of losses turns into Figure 3.

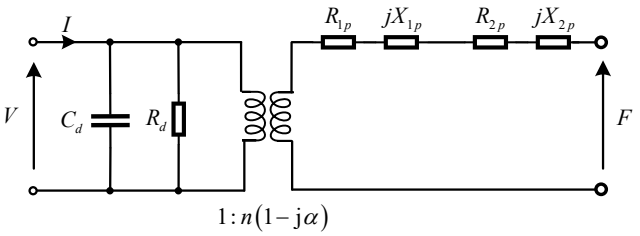

Figure 3. New decoupled electromechanical equivalent circuit model considering three types of losses.

III. EXPERIMENTAL AND SIMULATION RESULTS

A. EXPERIMENTAL TEST AND RESULTS

Piezoelectric ceramic disks (P-42, Hongsheng Acoustic Electronic Equipment Co., Ltd., Baoding, China) are fabricated with a radius of 10 mm and a thickness of 2 mm. The impedance magnitude and phase spectra of the actual samples are measured by the Precision Impedance Analyzer (E4990A, Keysight Technologies, Inc., Santa Rosa, CA), with specifications: the maximum voltage and current are 1 Vrms and 20 mArms, the impedance measurement accuracy is 0.5%. The experimental result of impedance spectra measured on disk specimens under 500 mV applied on the thickness 2 mm is shown in Figure 4. The resonance frequency is 110.20 kHz and antiresonance frequency is 123.67 kHz of the piezoelectric disk, in the first order radial vibration mode as marked in Figure 4.

This article has been accepted for publication in a future issue of this journal, but has not been fully edited. Content may change prior to final publication. Citation information: DOI 10.1109/ACCESS.2020.3028698, IEEE Access

TABLE I
MATERIALS PROPERTIES OF THE PIEZOELECTRIC CERAMIC

	Dielectric properties	Elastic properties		Piezoelectric properties	desnsity
Real parameter	$\varepsilon_{33}^{T}/\varepsilon_0$	s_{11}^{E} (m²/N)	s_{12}^{E} (m²/N)	d_{31} (C/N)	ρ (kg/m³)
	1200	12.6×10^{-12}	-3.78×10^{-12}	-108×10^{-12}	7600
Intensive loss	$\tan\delta_{33}^{'}$	$\tan\phi_{11}^{'}$	$\tan\phi_{12}^{'}$	$\tan\theta_{31}^{'}$	-
	0.0075	0.0021	0.0024	0.0056	-

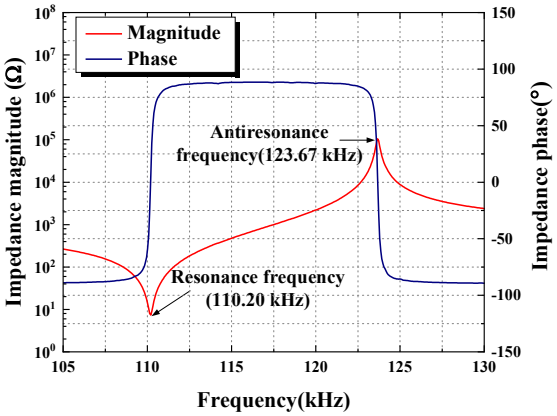

Figure 4. Experimental results of impedance spectra of the piezoelectric disk.

The definitions of the mechanical quality factors at resonance and antiresonance are depicted schematically in Figure 5 [21]. Q_R and Q_A are utilized to denote the quality factors at the resonance and antiresonance, respectively, as

$$Q_R = \frac{f_R}{f_{R2} - f_{R1}} \tag{28}$$

$$Q_A = \frac{f_A}{f_{A2} - f_{A1}} \tag{29}$$

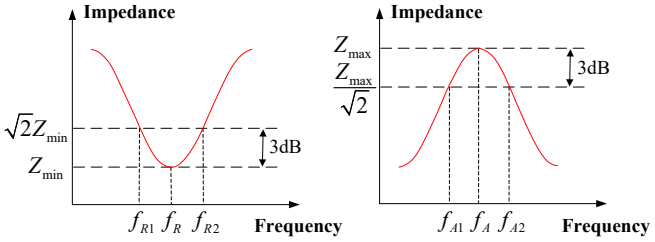

Figure 5. Definitions of mechanical quality factors at (a) resonance, (b) antiresonance.

Here, f_R is the resonance frequency; f_A is the antiresonance frequency; ($f_{R2} - f_{R1}$) and ($f_{A2} - f_{A1}$) correspond to the 3dB bandwidth around the resonance and antiresonance crests in the impedance curves, respectively.

The mechanical quality factors are calculated using the 3dB bandwidth method based on three times measurement results of the impedance spectra. Experimental results of mechanical quality factors are 485 ± 13 at resonance frequency and 638 ± 19 at antiresonance frequency.

B. SIMULATION RESULTS OF THE PIEZOELECTRIC DISK

In order to verify the accuracy of the proposed EC model, the configuration of the piezoelectric disk is simulated by MATLAB (Version R2017b, The MathWorks, Inc., Natick, Massachusetts). The essential material parameters of the piezoelectric ceramic disk used for the simulation are summarized in Table I. The real properties are measured and calculated according to the IEEE Standard [10]. The imaginary properties (i.e., intensive losses) are obtained by fitting the experimental impedance spectrum using the proposed EC model by MATLAB. It is notable that elastic losses are only related with the 3dB bandwidth at resonance frequency in impedance spectrum which could be directly determined, while the dielectric and piezoelectric losses are determined by 3dB bandwidth at both resonance and antiresonance frequencies in impedance spectrum which have to be determined after the determination of the elastic losses. When the piezoelectric disk vibrates freely, the two mechanical terminals of the proposed EC model in Figure 3 are short-circuited. Figure 6 is the comparison of the impedance spectrum simulating with considering three types of inherent losses and fixed small losses for comparison (which may be analogous to the loss-free material just to escape from the infinite divergence). The resonance and antiresonance frequencies are 110.46 kHz and 123.17 kHz in both impedance spectra. Three small losses are chosen as 0.1% of the three losses in order to demonstrate $Q_R = Q_A$ condition. It is obvious that the resonance and antiresonance frequencies are not affected by losses. However, the 3dB bandwidth of the impedance spectra exhibits a tremendous difference for inherent losses.

This article has been accepted for publication in a future issue of this journal, but has not been fully edited. Content may change prior to final publication. Citation information: DOI 10.1109/ACCESS.2020.3028698, IEEE Access

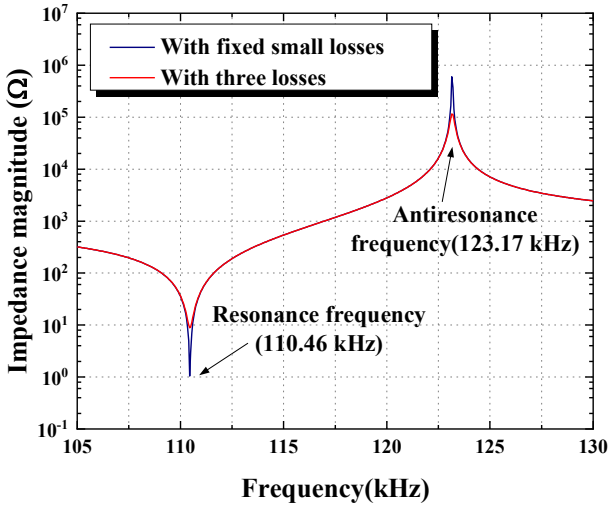

Figure 6. Simulation results of impedance with three losses and with fixed small losses.

Figure 7 show simulation results of mechanical quality factors at resonance and antiresonance frequencies as functions of three types of internal losses. It is clearly seen that Q_R is not affected by dielectric and piezoelectric loss factors, while it descends slightly with the increase of elastic loss factor. At the same time, Q_A descends with the rise of dielectric and elastic loss factors, while it ascends with the increase of piezoelectric loss factor. In conclusion, the mechanical quality factor at resonance Q_R only relates with the elastic loss factor in the radial vibration mode of the piezoelectric disk, while at antiresonance, the mechanical quality factor Q_A is determined by all the three loss factors. It is notable that $Q_R = Q_A$ when $\tan\theta'_{31} = \left(\tan\delta'_{33} + \tan\phi'_{11}\right)/2 \approx 0.0048$ in Figure 7 (c), which corresponds to the IEEE Standard model.

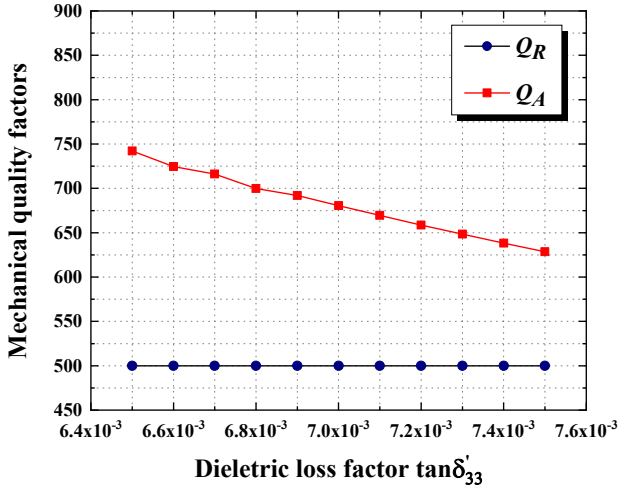

(a)

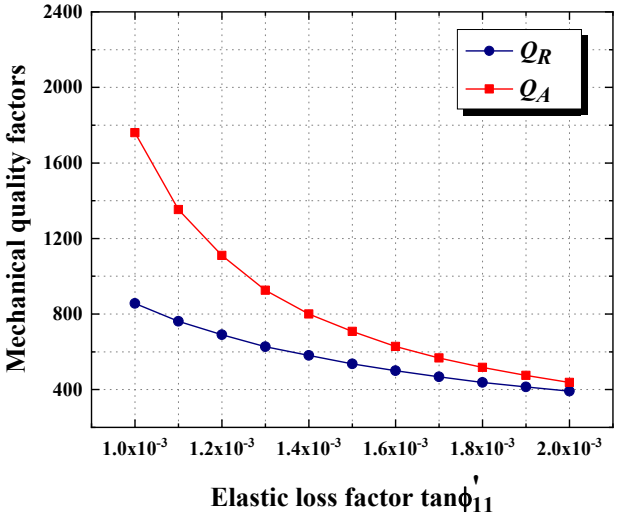

(b)

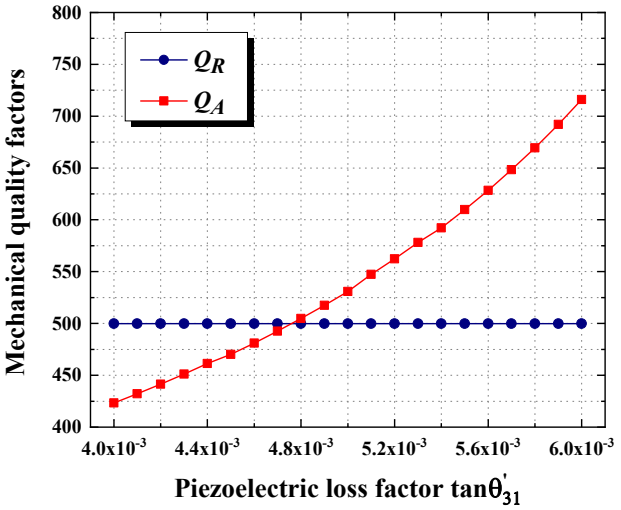

(c)

Figure 7. Simulation results of mechanical quality factors: (a) Q_R and Q_A with regard to dielectric loss factor; (b) Q_R and Q_A with regard to elastic loss factor; (c) Q_R and Q_A with regard to piezoelectric loss factor.

In the previous research, only dielectric and/or elastic losses are considered in EC models of piezoelectric disk in radial vibration. In order to verify the critical influence of the piezoelectric loss on the heat generation of piezoelectrics, the results of experiment, simulation with all three types of losses, and simulation without piezoelectric loss are compared and summarized in Table II. The deviation of the measured mechanical quality factors is less than 3%. It can be seen that $Q_R > Q_A$ without including the piezoelectric loss, which is entirely contradictory to the experimental results. By contrast, simulation with three types of losses have a much better agreement with the experimental results in the columns emphasized by gray shadow, which illustrates the significance of considering piezoelectric loss in equivalent circuit to the mechanical quality factor at antiresonance frequency.

This article has been accepted for publication in a future issue of this journal, but has not been fully edited. Content may change prior to final publication. Citation information: DOI 10.1109/ACCESS.2020.3028698, IEEE Access

TABLE II
RESULTS COMPARISON OF EXPERIMENT, SIMULATION WITH ALL THREE LOSSES AND SIMULATION WITHOUT PIEZOELECTRIC LOSS.

	Experiment	Three losses	Without piezo-loss
f_R(kHz)	110.20	110.46	110.46
f_A(kHz)	123.67	123.17	123.17
Q_R	485 ± 13	500	500
Q_A	638 ± 19	601	233

Similarly, the influence of relevant material properties on the resonance and antiresonance frequencies can be readily achieved utilizing the EC model. As shown in Figure 8, the resonance frequencies only show a downtrend with the growth of the elastic compliance, while the antiresonance frequencies decrease with the increase of relative permittivity, elastic compliance or piezoelectric constant. In addition, the relationship between the resonance or antiresonance frequencies and the structural parameters can be simulated. Here, we demonstrate the simulation results of resonance and antiresonance frequencies with regards to the radius of the piezoelectric disk by keeping the thickness t = 2 mm. As shown in Figure 9, both the resonance and antiresonance frequencies decrease linearly with the increase of the radius. To sum up, the simulation results using the EC model benefit the study of the heat generation and consequently the development of piezoelectric devices.

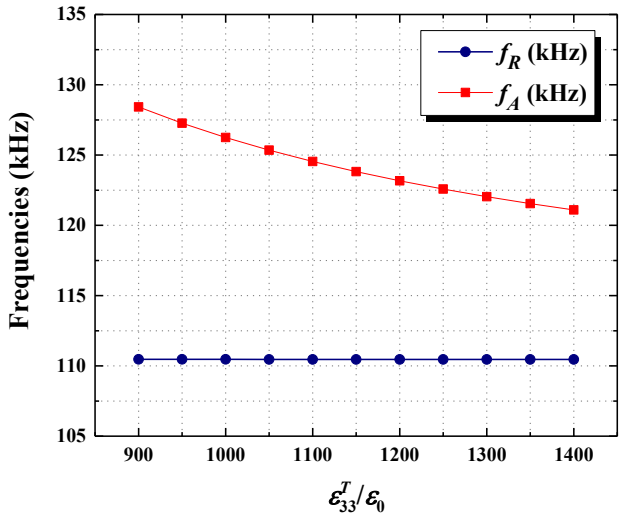

(a)

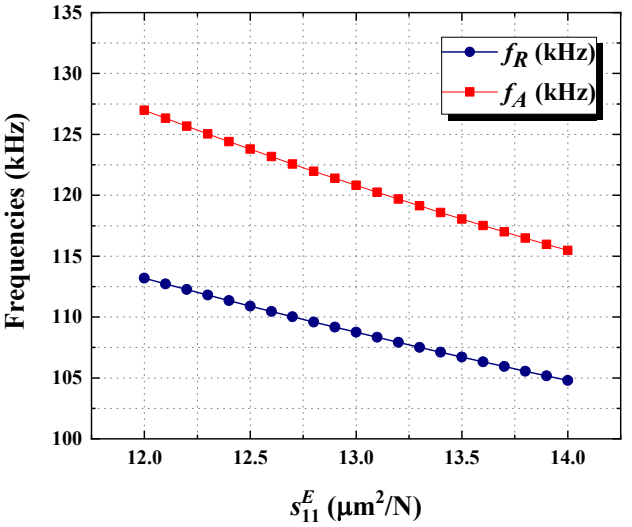

(b)

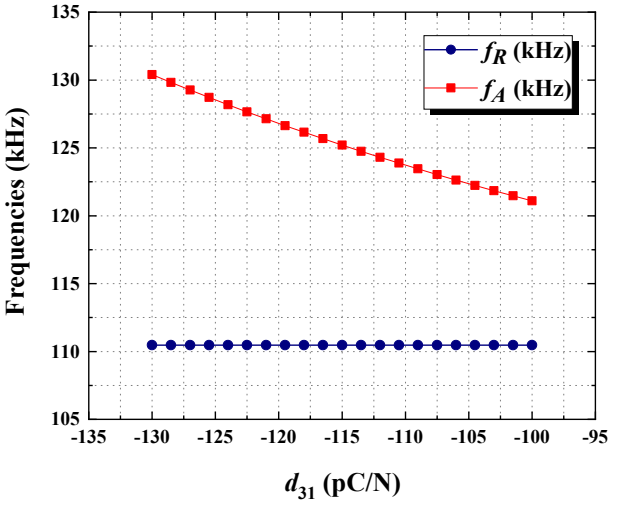

(c)

Figure 8. Simulation results of frequencies: (a) f_R and f_A as functions of relative permittivity; (b) f_R and f_A as functions of elastic compliance under constant electric field; (c) f_R and f_A as functions of piezoelectric constant.

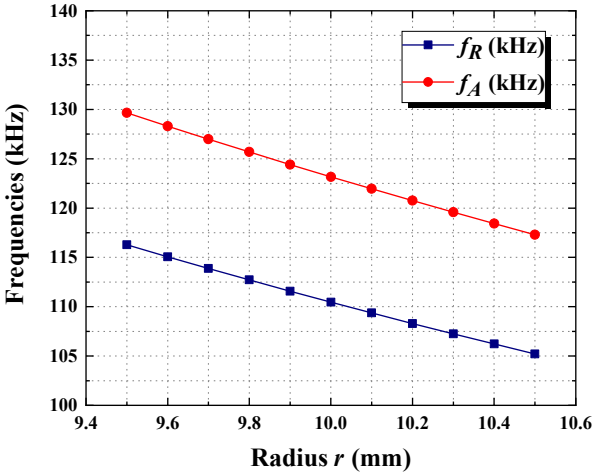

Figure 9. Frequencies f_R and f_A as functions of radius.

This article has been accepted for publication in a future issue of this journal, but has not been fully edited. Content may change prior to final publication. Citation information: DOI 10.1109/ACCESS.2020.3028698, IEEE Access

IV. CONCLUSION

In order to study the loss and heat generation in piezoelectric materials, this paper proposes a decoupled electromechanical EC model of a piezoelectric disk in radial vibration mode considering three types of internal losses. The EC model is utilized in simulation to obtain impedance spectra, and then the mechanical quality factors are calculated using the 3dB bandwidth method. A piezoelectric disk sample is fabricated and measured by experiment. Simulation results using the proposed EC model exhibit a better agreement with experimental results compared with the conventional model without piezoelectric losses, which verifies the importance of considering the piezoelectric loss for determining the mechanical quality factors (i.e., heat generation). Moreover, the proposed EC is an effective tool to study the influence of material properties and structural parameters on natural frequencies, which is beneficial for developing piezoelectric devices, such as ultrasonic motors, piezoelectric actuators, transducers and energy harvester, when utilizing a radial vibration mode of a piezoelectric disk.

REFERENCES

[1] X. Zhou, W. Chen, and J. Liu, "Novel 2-DOF Planar Ultrasonic Motor With Characteristic of Variable Mode Excitation," IEEE Trans. Ind. Electron., vol. 63, no. 11, pp. 6941–6948, Nov. 2016.
[2] Y. Liu, W. Chen, D. Shi, X. Tian, S. Shi, and D. Xu, "Development of a Four-Feet Driving Type Linear Piezoelectric Actuator Using Bolt-Clamped Transducers," IEEE Access, vol. 5, pp. 27162–27171, 2017.
[3] X. Yang, Y. Liu, W. Chen, and J. Liu, "Sandwich-Type Multi-Degree-of-Freedom Ultrasonic Motor With Hybrid Excitation," IEEE Access, vol. 4, pp. 905–913, 2016.
[4] K. Uchino, "Piezoelectric ultrasonic motors: overview," Smart Mater. Struct., vol. 7, no. 3, pp. 273–285, Jun. 1998.
[5] A. V. Mezheritsky, "Efficiency of excitation of piezoceramic transducers at antiresonance frequency," IEEE Transactions on Ultrasonics, Ferroelectrics, and Frequency Control, vol. 49, no. 4, pp. 484–494, Apr. 2002.
[6] H. N. Shekhani and K. Uchino, "Evaluation of the mechanical quality factor under high power conditions in piezoelectric ceramics from electrical power," Journal of the European Ceramic Society, vol. 35, no. 2, pp. 541–544, Feb. 2015.
[7] S. Sarangapani and X. Yan, "Improvement in the Electromechanical Properties of a Partially Diced Piezoelectric Disc Transducer," IEEE Access, vol. 6, pp. 70324–70330, 2018.
[8] B. Ju, Z. Guo, Y. Liu, G. Qian, L. Xu, and G. Li, "Self-Sensing Vibration Suppression of Piezoelectric Cantilever Beam Based on Improved Mirror Circuit," IEEE Access, vol. 7, pp. 148381–148392, 2019.
[9] K. Smyth and S.-G. Kim, "Experiment and simulation validated analytical equivalent circuit model for piezoelectric micromachined ultrasonic transducers," IEEE Transactions on Ultrasonics, Ferroelectrics, and Frequency Control, vol. 62, no. 4, pp. 744–765, Apr. 2015.
[10] "ANSI/IEEE Std 176-1987 An American National Standard IEEE Standard on Piezoelectricity," p. 74.
[11] K. Uchino, "Introduction to piezoelectric actuators: research misconceptions and rectifications," Jpn. J. Appl. Phys., vol. 58, no. SG, p. SG0803, Jul. 2019.
[12] Y. Park, Y. Zhang, M. Majzoubi, T. Scholehwar, E. Hennig, and K. Uchino, "Improvement of the standard characterization method on k33 mode piezoelectric specimens," Sensors and Actuators A: Physical, vol. 312, p. 112124, Sep. 2020.
[13] Shekhani Husain N. and Uchino Kenji, "Characterization of Mechanical Loss in Piezoelectric Materials Using Temperature and Vibration Measurements," Journal of the American Ceramic Society, vol. 97, no. 9, pp. 2810–2814, May 2014.
[14] X. Dong et al., "A new equivalent circuit for piezoelectrics with three losses and external loads," Sensors and Actuators A: Physical, vol. 256, pp. 77–83, Apr. 2017.
[15] X. Dong, C. Jiang, L. Jin, Z. Xu, and Y. Yuan, "Inherent Loss Analysis of Piezoelectrics in Radial Vibration and its Application in Ultrasonic Motor," IEEE Transactions on Ultrasonics, Ferroelectrics, and Frequency Control, vol. 67, no. 8, pp. 1632–1640, Aug. 2020.
[16] S. Lin, "Study on a new type of radial composite piezoelectric ultrasonic transducers in radial vibration," IEEE Transactions on Ultrasonics, Ferroelectrics, and Frequency Control, vol. 53, no. 9, pp. 1671–1678, Sep. 2006.
[17] S. Lin, L. Xu, and H. Wenxu, "A new type of high power composite ultrasonic transducer," Journal of Sound and Vibration, vol. 330, no. 7, pp. 1419–1431, Mar. 2011.
[18] Y. Huang and W. Huang, "An Improved Equivalent Circuit Model of Radial Mode Piezoelectric Transformer," IEEE Trans. Ultrason. Ferroelectr. Freq. Control, vol. 58, no. 5, pp. 1069–1076, May 2011.
[19] S. Lin, "Radial vibration of the combination of a piezoelectric ceramic disk and a circular metal ring," Smart Mater. Struct., vol. 16, no. 2, pp. 469–476, Feb. 2007.
[20] S. Lin, J. Hu, and Z. Fu, "Electromechanical characteristics of piezoelectric ceramic transformers in radial vibration composed of concentric piezoelectric ceramic disk and ring," Smart Mater. Struct., vol. 22, no. 4, p. 045018, Mar. 2013.
[21] K. Uchino, Y. Zhuang, and S. O. Ural, "Loss determination methodology for a piezoelectric ceramic: new phenomenological theory and experimental proposals," J. Adv. Dielect., vol. 01, no. 01, pp. 17–31, Jan. 2011.

XIAOXIAO DONG received the B.Sc. degree in electrical engineering from Nanjing Normal University, Nanjing, China, in 2012, and the Ph.D. degree in electrical engineering from Southeast University, Nanjing, China, in 2018.

From 2015 to 2016, she worked at the International Center for Actuators and Transducers, The Pennsylvania State University as a visiting scholar. Since 2018, she has been a Lecturer with the College of Energy and Electrical Engineering at Hohai University, Nanjing, China. Her research interests include ultrasonic motor developments related to materials, theoretical modeling and control technology, piezoelectric actuators, and energy harvesting.

KENJI UCHINO is Founding Director of International Center for Actuators and Transducers and Professor of EE and MatSE at Penn State University since 1991. He was Associate Director at The US Office of Naval Research – Global Tokyo Office, and also the Founder and Senior Vice President of Micromechatronics Inc., State College, PA. He was also awarded his MBA degree in 2008, and authored a textbook 'Entrepreneurship for Engineers'. He is a Fellow of American Ceramic Society and of IEEE, and also is a recipient of 31 awards, including International Ceramic Award from Global Academy of Ceramics (2016), IEEE-UFFC Ferroelectrics Recognition Award (2013).

His research interest is in solid state physics, especially in ferroelectrics and piezoelectrics, including basic research on theory, materials, device designing and fabrication processes, as well as application development of solid state actuators/sensors for precision positioners, micro-robotics, ultrasonic motors, smart structures, piezoelectric transformers and energy

harvesting. He has authored 582 papers, 78 books and 33 patents in the ceramic actuator area.

CHUNRONG JIANG was born in Fuzhou, China in 1983. She received the B.E., M.E., and Ph.D. degrees in Electrical Engineering from Southeast University, China, in 2006, 2009, and 2013, respectively.

From 2011 to 2012, she worked at the Department of Mechanical and Aerospace Engineering, Missouri University of Science and Technology, USA, as a visiting scholar. She is currently an associate professor of Electrical Engineering at Nanjing Institute of Technology, China. Her research field is modeling and control of piezoelectric ultrasonic motors.

LONG JIN received his Ph.D. degree from Nanjing University of Aeronautics and Astronautics, Nanjing, China, in 1997.

He has been a Professor of Electrical Engineering at Southeast University since 2003. His research interest is in ultrasonic motors, high power electronics technology, and robot design.

ZHIKE XU received his Ph.D. degree from Southeast University, Nanjing, China, in 2005.

He is currently an associate professor at School of Electrical Engineering, Southeast University. His research interests include numerical modeling of ultrasonic motors, and piezoelectric actuators.

YUE YUAN received the B.Sc. and M.Sc. degrees in electrical engineering from Xi'an Jiaotong University, Xi'an, China, in 1987 and 1990, respectively, and the Ph.D. degree from Hiroshima University, Hiroshima, Japan, in 2002.

He joined the faculty of Xi'an Jiaotong University in 1990. He was with Hiroshima University from 1998 to 2002. In 2003, he joined Hohai University as a Professor. He was the former dean of the College of Energy and Electrical Engineering, Hohai University, Nanjing, China. His recent research interests include power system operations and control, renewable energy and distributed generation, smart grid and micro grid.